

Supporting Information

Pressure-stabilized Hexafluorides of First-row Transition

Metals

Jianyan Lin^{1,2‡}, Qiuping Yang^{1,3‡}, Xing Li[‡], Xiaohua Zhang^{1,3}, Fei Li¹ and Guochun Yang^{1,3,*}

¹State Key Laboratory of Metastable Materials Science & Technology and Key Laboratory for Microstructural Material Physics of Hebei Province, School of Science, Yanshan University, Qinhuangdao 066004, China

²College of Physics, Changchun Normal University, Changchun 130032, China

³Centre for Advanced Optoelectronic Functional Materials Research and Key Laboratory for UV Light-Emitting Materials and Technology of Ministry of Education, Northeast Normal University, Changchun 130024, China

*Address correspondence to: yanggc468@nenu.edu.cn; yanggc@ysu.edu.cn

Index	Page
1. Computational details	S1
2. Calculated Birch-Murnaghan equation of states for FeF ₄ with <i>Cmca</i> symmetry	S3
3. Phase stabilities of Fe-F compounds at high pressures	S4
4. Phonon dispersion curves for the predicted compounds	S4
5. Volume variations of different FeF ₆ phases	S5
6. <i>U</i> and <i>PV</i> curves of different FeF ₆ phases	S5
7. Electron localization function of <i>R-3</i> FeF ₆	S6
8. Phase stabilities of Sc-F, Ti-F, V-F, Cr-F, and Mn-F systems	S6
9. Crystal structures of CrF ₆ and MnF ₆	S6
10. Electronic band structure and corresponding PDOS	S7
11. The energy difference between TM 3d and F 2p orbital	S7
12. Validation of the reliability of the used methodology	S8

13. The magnetic moment of the Fe-F, Co-F, and Ni-F phases.....	S8
14. The calculated lattice parameters of FeF ₃ , CoF ₃ , and NiF ₃ at 1 atm.....	S9
15. The crystal structural information of the predicted stable phases.....	S10
16. References	S13

Computational Details

Our structural prediction approach is based on a global minimization of free energy surfaces merging *ab initio* total-energy calculations with CALYPSO (Crystal structure AnaLYsis by Particle Swarm Optimization) methodology as implemented in the CALYPSO code.^{1,2} The structures of various TM-F compositions were searched at 300 GPa, with the simulation cell sizes of 1 – 4 formula units (f.u.) for TMF_x ($x = 1 - 4$) and 1 – 2 formula units (f.u.) for TMF_x ($x = 5 - 8$). In the first step, random structures with certain symmetry are constructed in which atomic coordinates are generated by the crystallographic symmetry operations. Local optimizations using the VASP code³ were done with the conjugate gradients method and stopped when total energy changes became smaller than 1×10^{-5} eV per cell. After processing the first generation structures, 60% of them with lower enthalpies are selected to construct the next generation structures by PSO (Particle Swarm Optimization). 40% of the structures in the new generation are randomly generated. A structure fingerprinting technique of bond characterization matrix is applied to the generated structures, so that identical structures are strictly forbidden. These procedures significantly enhance the diversity of the structures, which is crucial for structural global search efficiency. In most cases, structural searching simulations for each calculation were stopped after generating 1000 ~ 1200 structures (e.g., about 20 ~ 30 generations).

Structural optimization and electronic structure calculations were performed with the framework of density functional theory (DFT)^{4,5} within the Perdew-Burke-Ernzerhof (PBE)⁶ functional of the generalized gradient approximation (GGA),⁷ as implemented by the VASP (Vienna *Ab initio* Simulation Package) code. The all-electron projector augmented-wave (PAW)⁸ pseudopotentials of Sc, Ti, V, Cr, Mn, Fe, Co, Ni, and F treat $3d^14s^2$, $3d^24s^2$, $3d^34s^2$, $3d^54s^1$, $3d^54s^2$, $3d^64s^2$, $3d^74s^2$, $3d^84s^2$ and $2s^22p^5$ electrons as the valence electrons, respectively. The cutoff energy was set at 800 eV, and Monkhorst-Pack scheme⁹ with a k -point grid of $2\pi \times 0.03 \text{ \AA}^{-1}$ in Brillouin zone was selected to ensure that all enthalpy calculations converged to less than 1 meV per atom. The dynamical stability of predicted structures was determined by

phonon calculations using a supercell approach with the finite displacement method¹⁰ as implemented in the Phonopy code.¹¹ Crystal orbital Hamilton population (COHP) analysis giving the information on the interatomic interaction was implemented in the LOBSTER package.^{12,13} The electron localization function (ELF)¹⁴ was calculated using VASP code.

Supplementary Figures

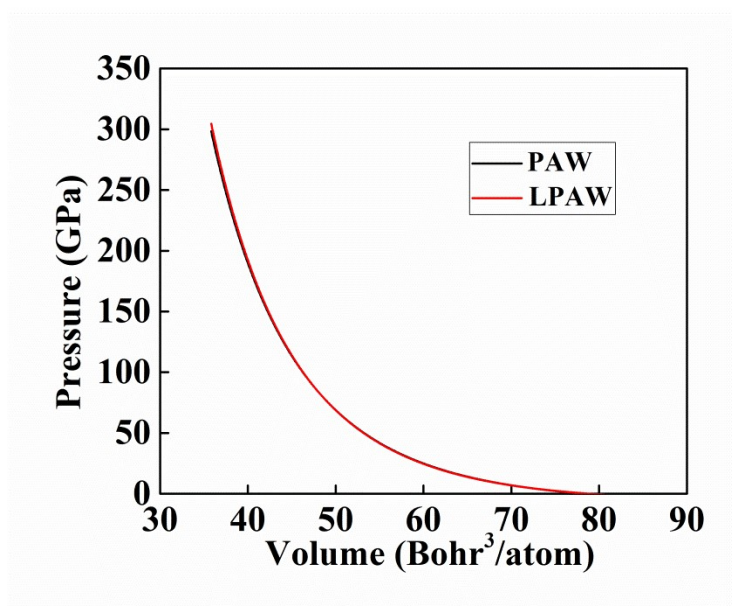


Figure S0. Comparison of the fitted Birch-Murnaghan equation of states for FeF₄ with *Cmca* symmetry by using the calculated results from the PAW pseudopotentials and the full-potential LAPW methods.

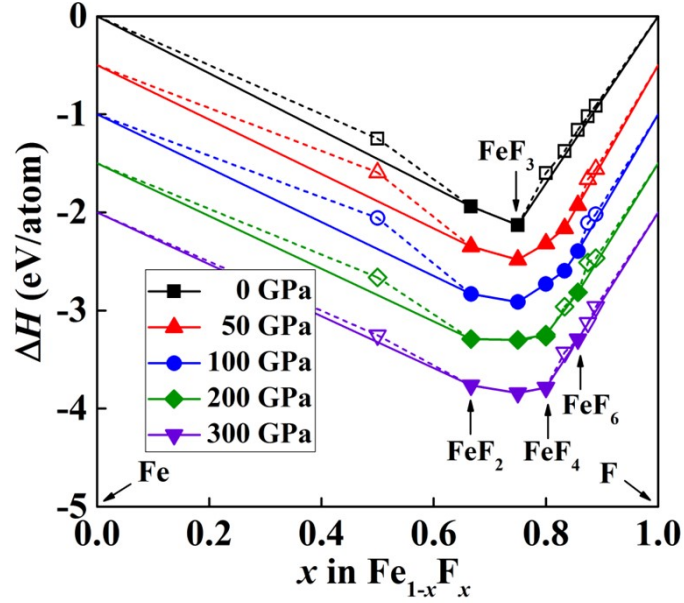


Figure S1. Phase stabilities of various FeF_x ($x = 1-8$) compounds with respect to elemental Fe and F_2 solids at the different pressures. The elemental Fe solid with bcc and hcp structures,¹⁵ and the $C2/c$ ¹⁶ and $Cmca$ ¹⁷ phases of elemental F_2 solids were adopted in the enthalpy of formation calculations. For clarity, we have offset the formation enthalpies of each composition by -0.5, -1.0, -1.5, and -2.0 at 50, 100, 200, and 300 GPa, respectively.

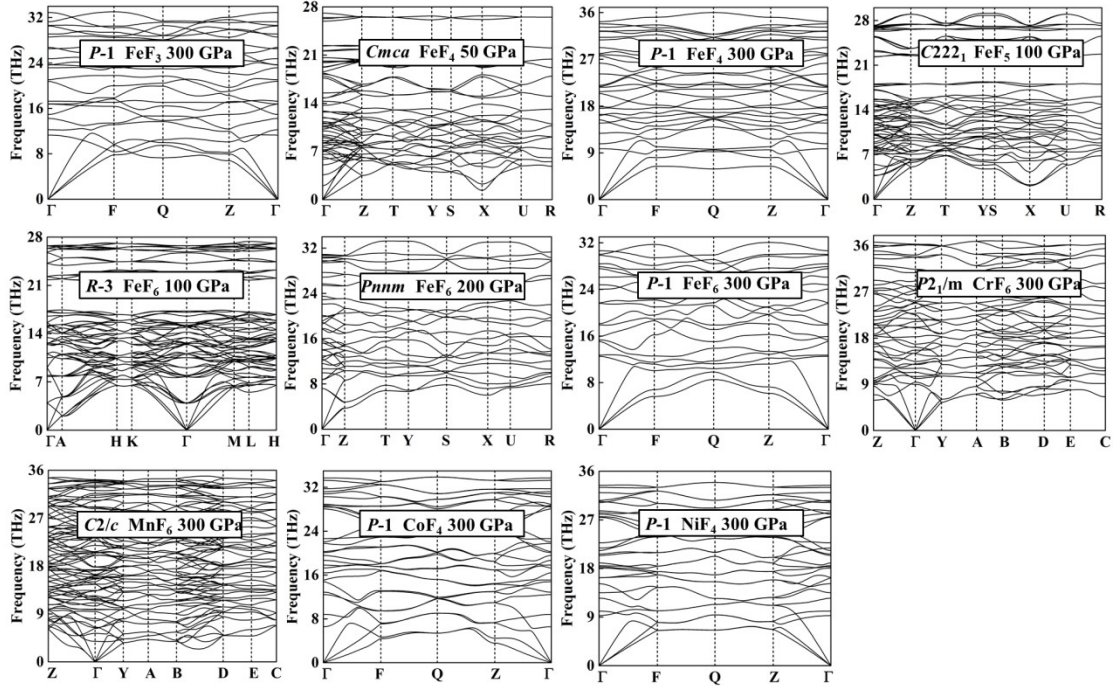


Figure S2. Phonon dispersion curves of the predicted Fe-F binary compounds: CrF_6 , MnF_6 , CoF_4 , and NiF_4 . The absence of any imaginary frequency modes in the first

Brillouin zone indicates the dynamical stability of the predicted compounds.

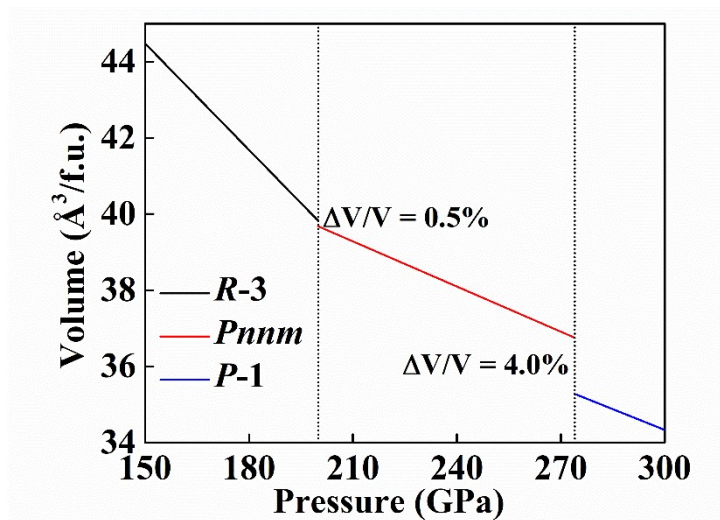


Figure S3. Calculated volume variations as a function of pressure for the *R-3*, *Pnnm* and *P-1* FeF_6 .

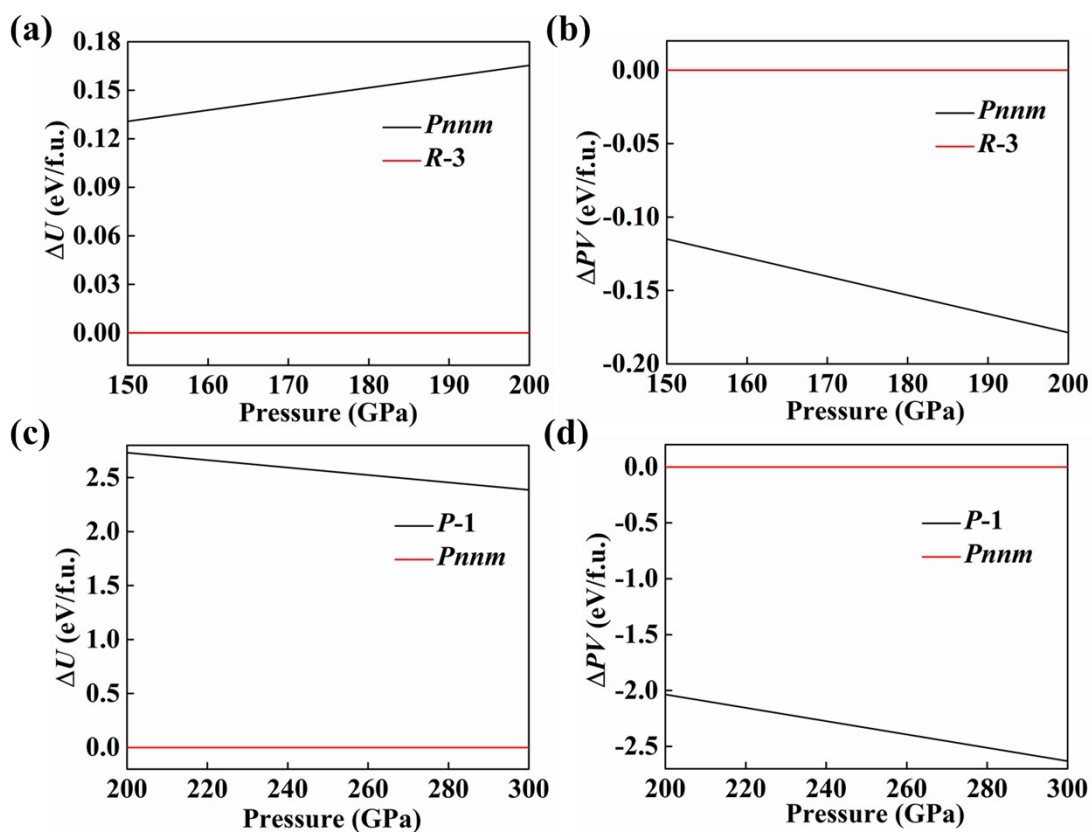


Figure S4. (a) U and (b) PV curves for *Pnnm* FeF_6 relative to *R-3* FeF_6 (c) U and (d) PV curves for *P-1* FeF_6 relative to *Pnnm* FeF_6 .

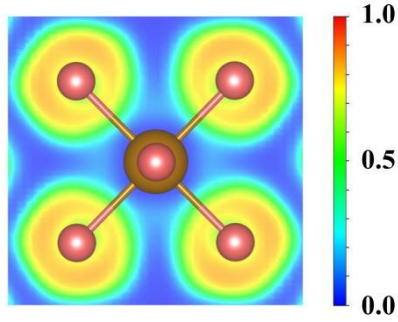


Figure S5. Electron localization function of $R\text{-}3 \text{ FeF}_6$ at 100 GPa in $(2.02 -1 4.07)$ plane. In general, the large ELF values (> 0.5) correspond to the lone electron pairs, core electrons, or covalent bonds, whereas the ionic bonds are represented by smaller ELF values (< 0.5).

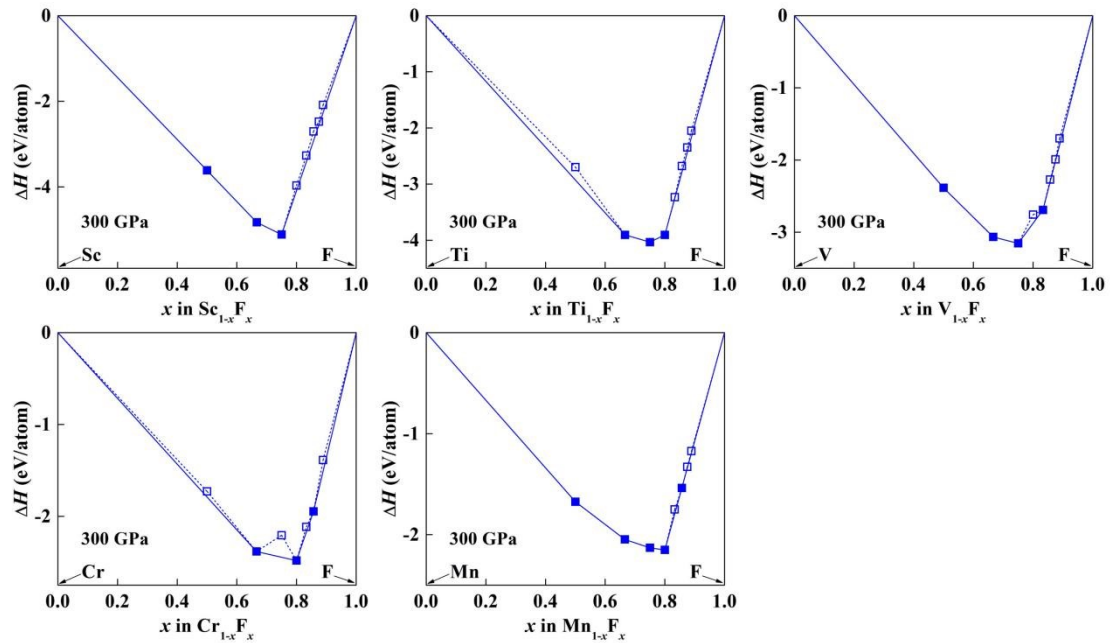


Figure S6. Phase stabilities of the considered Sc-F, Ti-F, V-F, Cr-F, and Mn-F compounds with respect to elemental Sc, Ti, V, Cr, Mn and F_2 solids at 300 GPa.

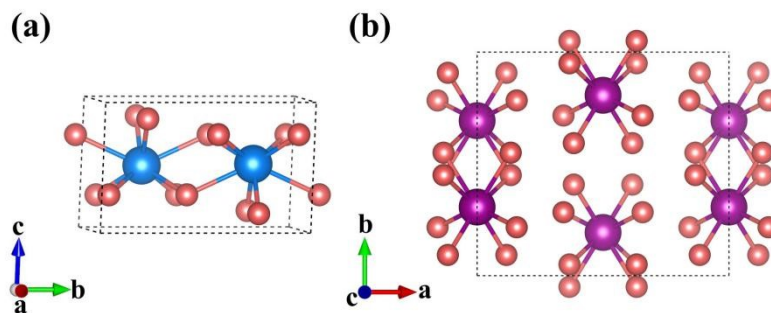


Figure S7. Crystal structures of (a) $P2_1/m \text{ CrF}_6$ and (b) $C2/c \text{ MnF}_6$ at 300 GPa. Both

of the center metal atoms are eight-coordinated with F atoms, forming edge-sharing polyhedrons.

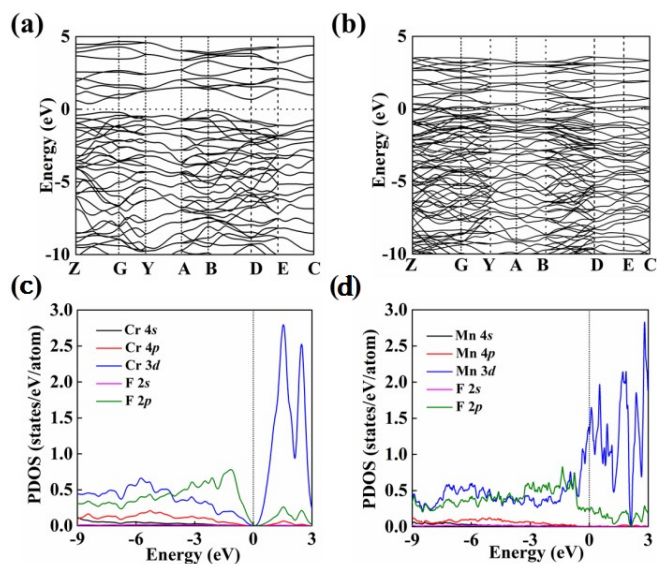


Figure S8. Electronic band structure and corresponding PDOS for (a, c) $P2_1/m$ CrF_6 , (b, d) $C2/c$ MnF_6 at 300 GPa.

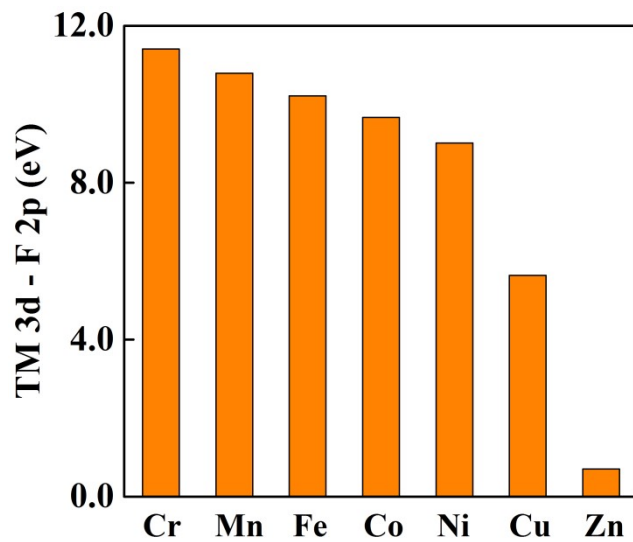


Figure S9. The energy difference between TM 3d and F 2p orbital at 300 GPa (M = Cr, Mn, Fe, Co, Ni, Cu, and Zn).

Supplemental Tables

Table. S1. Comparison of the transition pressure (GPa) of MgF₂.

Transition pressure (GPa)	Rutile→CaCl	CaCl ₂ →PdF ₂	PdF ₂ →Cotunnite
Calculation by V. Kanchana et al. ¹⁸	10.0	15.4	36.8
Experiment by J. Haines et al. ¹⁹	9.1	14	36
Our PBE-GGA calculated results	7.0	15.2	45.4

Table. S2. The magnetic moment of the Fe-F, Co-F, and Ni-F phases.

	Phases	Pressure (GPa)	Fe/Co/Ni Magnetic moment (μ_B /atom)	Anti-ferromagnetic (AFM) or ferromagnetic (FM)
FeF ₂	<i>P4₂/mnm</i>	0.0001	3.57	AFM
	<i>Pnma</i>	300	3.33	AFM
FeF ₃	<i>R-3c</i>	0.0001	4.03	AFM
	<i>P-1</i>	300	0.0	-
FeF ₄	<i>Cmca</i>	100	1.70	AFM
	<i>P-1</i>	300	0.0	-
FeF ₅	<i>C222₁</i>	100	1.96	AFM
	<i>R-3</i>	100	1.56	FM
FeF ₆	<i>Pnnm</i>	200	1.30	FM
	<i>P-1</i>	300	0.0	-
CoF ₂	<i>P-3m1</i>	300	1.25	AFM
CoF ₃	<i>C2/c</i>	300	0.0	-
CoF ₄	<i>P-1</i>	300	0.63	FM
NiF ₂	<i>P-3m1</i>	300	1.54	FM
NiF ₃	<i>C2/c</i>	300	0.0	-
NiF ₄	<i>P-1</i>	300	0.0	-

Table. S3. The calculated lattice parameters of FeF₃, CoF₃, and NiF₃, compared with previous works.

Phases	pressure	Lattice Parameters (Å, °) (in our work)	Lattice Parameters (Å, °) (in other works)^{20,21,22}
<i>R-3c-FeF₃</i>	1 atm	$a = 5.265$	$a = 5.195$
		$b = 5.265$	$b = 5.194$
		$c = 13.579$	$c = 13.335$
<i>R-3c-CoF₃</i>	1 atm	$a = 5.109$	$a = 5.035$
		$b = 5.109$	$b = 5.035$
		$c = 13.213$	$c = 13.219$
<i>R-3c-NiF₃</i>	1 atm	$a = 4.912$	$a = 4.809$
		$b = 4.912$	$b = 4.809$
		$c = 13.043$	$c = 13.067$

Table. S4. Structural information of the predicted stable Fe-F phases.

Phases	Pressure (GPa)	Lattice Parameters (Å, °)	Atoms	Wyckoff Positions (fractional)		
				<i>x</i>	<i>y</i>	<i>z</i>
<i>P</i> -1 FeF ₃	300	<i>a</i> = 2.8959	Fe(2i)	0.63763	1.27520	0.20164
		<i>b</i> = 3.5736	F(2i)	1.13832	1.27655	0.97159
		<i>c</i> = 4.4116	F(2i)	1.13497	1.26988	0.42766
		α = 102.5063	F(2i)	0.59436	1.18866	0.69742
		β = 90.0128 γ = 113.8800				
<i>Cmca</i> FeF ₄	100	<i>a</i> = 4.9929	Fe (4b)	0.00000	1.00000	0.50000
		<i>b</i> = 8.0109	O(8f)	0.00000	1.33797	1.27327
		<i>c</i> = 3.9594	O(8e)	0.25000	0.89735	0.75000
		α = 90.0000				
		β = 90.0000 γ = 90.0000				
<i>P</i> -1 FeF ₄	300	<i>a</i> = 3.6993	Fe(1h)	0.50000	0.50000	0.50000
		<i>b</i> = 3.8317	Fe(1d)	0.50000	0.00000	0.00000
		<i>c</i> = 3.8329	F(2i)	0.22683	0.25840	0.24173
		α = 89.6046	F(2i)	0.21040	0.74592	0.37711
		β = 76.4343	F(2i)	0.21039	0.12294	0.75416
	γ = 103.5114	F(2i)	0.22343	0.62938	0.87080	
<i>C222</i> ₁ FeF ₅	100	<i>a</i> = 3.8855	Fe(4b)	0.00000	0.11269	1.25000
		<i>b</i> = 11.4696	F(4a)	0.80457	0.00000	0.50000
		<i>c</i> = 3.6791	F(8c)	0.18397	0.20753	0.97384
		α = 90.0000	F(8c)	0.34601	0.89985	1.48462
		β = 90.0000 γ = 90.0000				
<i>R</i> -3 FeF ₆	100	<i>a</i> = 3.8810	Fe(3a)	0.00000	0.00000	0.00000
		<i>b</i> = 3.8810	F(18f)	0.97624	0.66435	0.57843
		<i>c</i> = 10.7468				
		α = 90.0000				
		β = 90.0000 γ = 120.0000				
<i>Pnmm</i> FeF ₆	200	<i>a</i> = 3.4295	Fe(2b)	0.00000	0.00000	0.50000
		<i>b</i> = 3.7015	F(8h)	0.70913	0.82232	0.67867
		<i>c</i> = 6.2530	F(4g)	0.25889	0.63263	0.50000
		α = 90.000				
		β = 90.000 γ = 90.000				
<i>P</i> -1 FeF ₆	300	<i>a</i> = 2.9668	Fe(1b)	0.00000	0.00000	0.50000
		<i>b</i> = 3.5459	F(2i)	0.44303	0.26665	0.62154
		<i>c</i> = 3.5754	F(2i)	0.12167	0.38082	0.22897

$\alpha = 98.0210$ F(2i) 0.74081 0.16157 0.00418
 $\beta = 67.1887$
 $\gamma = 92.0942$

Table. S5. Structural information of the predicted stable M-F (M=Cr, Mn, Co, and Ni) phases.

Phases	Pressure (GPa)	Lattice Parameters (Å, °)	Atoms	Wyckoff Positions (fractional)		
				<i>x</i>	<i>y</i>	<i>z</i>
<i>P2₁/m</i> CrF ₆	300	<i>a</i> = 4.0962	Cr(2e)	0.64791	0.75000	0.51215
		<i>b</i> = 5.3007	F(2e)	0.01210	0.25000	0.85198
		<i>c</i> = 3.4226	F(2e)	0.45124	0.75000	1.14679
		<i>α</i> = 90.0000	F(4f)	0.83671	0.94123	0.74597
		<i>β</i> = 74.3909 <i>γ</i> = 90.0000	F(4f)	0.69477	0.06509	1.27890
<i>C2/c</i> MnF ₆	300	<i>a</i> = 6.9141	Mn(4e)	0.50000	0.80681	0.25000
		<i>b</i> = 5.8112	F(8f)	0.15709	0.21634	-0.34588
		<i>c</i> = 3.6977	F(8f)	0.11621	0.90734	-0.39017
		<i>α</i> = 90.0000	F(8f)	0.36664	0.94994	-0.48781
		<i>β</i> = 108.586 <i>γ</i> = 90.0000				
<i>P-1</i> CoF ₄	300	<i>a</i> = 3.5253	Co(1e)	0.50000	0.50000	0.00000
		<i>b</i> = 3.7594	Co(1f)	0.50000	0.00000	0.50000
		<i>c</i> = 3.8853	F(2i)	0.29352	0.87294	0.90159
		<i>α</i> = 89.9805	F(2i)	0.70636	0.37280	0.59850
		<i>β</i> = 80.2394 <i>γ</i> = 90.0114	F(2i)	0.14423	0.34507	0.81797
<i>P-1</i> NiF ₄	300	<i>a</i> = 3.5346	Ni(1e)	0.50000	0.50000	0.00000
		<i>b</i> = 3.7677	Ni(1f)	0.50000	0.00000	0.50000
		<i>c</i> = 3.8515	F(2i)	0.29689	0.87403	0.89857
		<i>α</i> = 90.0112	F(2i)	0.70320	0.37417	0.60140
		<i>β</i> = 82.0651 <i>γ</i> = 90.0110	F(2i)	0.13839	0.34330	0.82119
	F(2i)	0.13838	0.15651	0.32113		

References

1. Y. Wang, J. Lv, L. Zhu and Y. Ma, *Phys. Rev. B*, 2010, **82**, 094116.
2. Y. Wang, J. Lv, L. Zhu and Y. Ma, *Comput. Phys. Commun.*, 2012, **183**, 2063-2070.
3. G. Kresse and J. Furthmüller, *Phys. Rev. B*, 1996, **54**, 11169-11186.
4. P. Hohenberg and W. Kohn, *Phys. Rev.*, 1964, **136**, B864-B871.
5. W. Kohn and L. J. Sham, *Phys. Rev.*, 1965, **140**, A1133-A1138.
6. J. P. Perdew, K. Burke and M. Ernzerhof, *Phys. Rev. Lett.*, 1996, **77**, 3865-3868.
7. J. P. Perdew, J. A. Chevary, S. H. Vosko, K. A. Jackson, M. R. Pederson, D. J. Singh and C. Fiolhais, *Phys. Rev. B*, 1992, **46**, 6671-6687.
8. P. E. Blöchl, *Phys. Rev. B*, 1994, **50**, 17953-17979.
9. H. J. Monkhorst and J. D. Pack, *Phys. Rev. B*, 1976, **13**, 5188-5192.
10. K. Parlinski, Z. Q. Li and Y. Kawazoe, *Phys. Rev. Lett.*, 1997, **78**, 4063-4066.
11. A. Togo, F. Oba and I. Tanaka, *Phys. Rev. B*, 2008, **78**, 134106.
12. R. Dronskowski and P. E. Bloechl, *J. Phys. Chem.*, 1993, **97**, 8617-8624.
13. S. Maintz, V. L. Deringer, A. L. Tchougréeff and R. Dronskowski, *J. Comput. Chem.*, 2016, **37**, 1030-1035.
14. A. D. Becke and K. E. Edgecombe, *J. Chem. Phys.*, 1990, **92**, 5397-5403.
15. D. Alfè, G. Kresse and M. J. Gillan, *Phys. Rev. B*, 2000, **61**, 132-142.
16. L. Pauling, I. Keaveny and A. B. Robinson, *J. Solid State Chem.*, 1970, **2**, 225-227.
17. Q. Lv, X. Jin, T. Cui, Q. Zhuang, Y. Li, Y. Wang, K. Bao and X. Meng, *Chin. Phys. B*, 2017, **26**, 076103.
18. V. Kanchana, G. Vaitheeswaran and M. Rajagopalan, *J. Alloys Compd.*, 2003, **352**, 60-65.
19. J. Haines, J. M. Léger, F. Gorelli, D. D. Klug, J. S. Tse and Z. Q. Li, *Phys. Rev. B*, 2001, **64**, 134110.
20. M. Leblanc, J. Pannetier, G. Ferey and R. De Pape, *Revue de chimie minérale*, 1985, **22**, 107-114.
21. M. A. Hepworth, K. H. Jack, R. D. Peacock and G. J. Westland, *Acta Crystallogr.*, 1957, **10**, 63-69.
22. B. Zemva, K. Lutar, L. Chacon, M. Fele-Beuermann, J. Allman, C. Shen and N. Bartlett, *J. Am. Chem. Soc.*, 1995, **117**, 10025-10034.